Angular-momentum transfer due to postcollision interaction in atomic inner ns^2 -shell photoionization

L. Gerchikov*
Department of Experimental Physics, Peter the Great St. Petersburg Polytechnic University, 195251 St. Petersburg, Russia

R. Guillemin and M. Simon
Sorbonne Universités, UPMC Univ Paris 06, UMR 7614, Laboratoire de Chimie Physique Matière et Rayonnement, F-75005, Paris, France and CNRS, UMR 7614, Laboratoire de Chimie Physique Matière et Rayonnement, F-75005, Paris, France

S. Sheinerman†
Department of Physics, St. Petersburg State Maritime Technical University, 190121 St. Petersburg, Russia
(Received 3 January 2017; revised manuscript received 19 May 2017; published 29 June 2017)

A concrete mechanism of angular-momentum transfer in photoionization process is proposed for electron photoemission from deep inner atomic shells. It is demonstrated that the leading contribution to angular-momentum transfer is provided by postcollision interaction of the photoelectrons and Auger electrons. The standard theoretical approach to postcollision interaction has been considerably improved by taking into account angular-momentum transfer. The theory developed is applied to the photoionization of $1s^2$ shell in Ar. Calculations show the noticeable influence of angular-momentum transfer on the photoelectron angular distribution.

DOI: 10.1103/PhysRevA.95.063425

I. INTRODUCTION

Photoionization of an inner atomic shell is followed by different decay processes of the inner vacancy. The dynamics of the decay can be rather complicated, although in the simplest case it is reduced to the ordinary single Auger decay that leads to the emission of an Auger electron and creation of two vacancies in an outer shell. Coulomb interaction between the photoelectron, the Auger electron, and the ion of the atomic target is known as postcollision interaction (PCI). PCI leads to distortion of the energy and angular distributions of the emitted photoelectrons and Auger electrons, which has been widely investigated during the last few decades (see, e.g., reviews [1,2]). In the classical picture, PCI distortion of the energy distribution implies an energy exchange between the emitted Auger, photoelectrons, and residual ion whereas distortion of the angular distribution means that the photoelectrons and Auger electrons change direction during their emission. Generally speaking, one can expect the emitted electrons to exchange also the angular momentum due to the PCI. Such an exchange can also lead to modifying the electron emission angular pattern.

In the past years, the attention of the investigators was mainly drawn to the study of the energy distribution of the emitted particles. A novel manifestation of PCI distortion in the spectra of the photoelectrons and Auger electrons was considered in the case of single, double, and multiple Auger decay processes both theoretically and experimentally [3–10]. The manifestation of PCI on electron angular distributions has been much less documented. Angular-dependent photoionization cross sections distorted by PCI were obtained within the semiclassical [6,11] and eikonal [12,13] approaches. These models predict a strong PCI influence on the angular distribution of the photoelectrons and Auger electrons under condition of low relative velocity of the escaping electrons [14] in the case of electron-electron coincidence experiments. It should be noted that the semiclassical and eikonal models rely upon the assumption that the emitted electrons are far apart and their trajectories are a straight line, which is justified under many real experimental conditions. The direct Coulomb interaction between the photoelectrons and Auger electrons, which is taken into account more or less precisely in these models, leads to PCI distortion of the angular distribution of the emitted electrons. The theoretical predictions were confirmed by recent coincidence measurements [15,16]. However, in the case of noncoincidence measurements, when only the angular distribution of the photoelectrons is recorded, the PCI distorted factor being considered within the semiclassical and eikonal approaches proves to be equal to 1 [14,17]. In other words, within theses approximations the influence of Auger electrons on the photoelectron angular distribution disappears with averaging over all directions of Auger emission. It follows that these approaches do not allow describing correctly the angular-momentum exchange and more accurate quantum mechanical treatment should be employed.

In the case of near-threshold photoionization of a deep atomic shell followed by a single Auger decay, the exiting PCI theories predict negligible photoemission angular distortion: photoionization results in the creation of a low-energy photoelectron and a fast Auger electron, which leaves quickly the reaction zone. Therefore, the PCI energy distortion is determined mostly by the interaction of the slow photoelectron with the ionic field, which varies in the course of the Auger decay of the inner vacancy. The interaction between the photoelectrons and Auger electrons plays a minor role. That is why numerous quantum mechanical models considering the PCI problem as a two-body problem [18–23] are adequate in this case for the description of PCI distorted energy distribution.

*lgerchikov@mail.ru
†sergei.sheinerman@gmail.com

The amplitude of the process considered within these models is proportional to the overlap integral between the wave functions of the slow electron moving in fields of the intermediate and the final ionic states. In the intermediate state, prior to Auger decay, the photoelectron propagates in the field of a singly charged ion whereas after Auger decay (in the final state) it moves in the field of a doubly charged ion. In first approximation, the models neglect the influence of the Auger electron on the photoelectron. Thus, the photoelectron is considered as having a constant value of angular momentum. Hence, the angular distribution of the photoelectron is determined by the angular momentum of the ionized shell, e.g., in the case of inner ns^2 ionization the photoelectron is a p electron ($l = 1$). In the case of linearly polarized photons, the photoelectron angular distribution can be written [24] $d\sigma/d\Omega = \sigma/(4\pi)\,[1 + \beta\, P_2(\cos\theta)]$, where σ is the total cross section, θ is the angle between the axis of linear polarization of the incident photon and the direction of the outgoing photoelectron, and β is the asymmetry parameter. For ns^2-shell photoionization, the value of the asymmetry parameter is equal to $\beta = 2$ [25]. Accounting for Coulomb interaction between the fast Auger electron and the slow photoelectron within the semiclassical and eikonal approaches [14,17] does not change this result because of the assumption of straight line electron trajectories. Such an approach neglects angular-momentum transfer.

As far as we know, there was only one attempt to take into account the possibility of angular-momentum exchange for slow photoelectrons [26]. The authors assumed that the angular momentum of the outgoing photoelectron in the final state differs from its value in the intermediate state in order to explain the structures observed in the measured energy spectra of the emitted photoelectron [27,28]. However, no specific physical mechanism of angular-momentum exchange has been considered.

There are several known mechanisms of angular-momentum transfer in photoionization processes [25,29], e.g., a rearrangement of the open outer shells of the ion, intershell electron correlation, and the photoelectron scattering on the anisotropic field of the ion. The latter has been reported to affect the asymmetry parameter β in the photoionization of the outer atomic s shells [25]. In inner-shell atomic photoionization followed by Auger decay considered here, the role of intershell correlations seems to be negligible because of the large energy difference between the ionized deep ns^2 shell and other subshells. At the same time, a different source of angular-momentum exchange appears, namely the interaction between Auger and photoelectrons.

The goal of the present paper is to reveal the leading mechanism of angular-momentum transfer due to PCI in deep inner-shell ionization and estimate its effect on the asymmetry parameter β at the photoionization threshold. For this purpose, we have developed a quantum mechanical theory of PCI, which accounts for the angular-momentum exchange due to interaction of the photoelectron with both the Auger electron and the residual ion. Due to the large velocity of the Auger electron, its interaction with the slow photoelectron is treated perturbationally. In zeroth approximation our approach coincides with the existing PCI two-body theories [18–23]. In the first Born approximation, we obtain a nonzero angular-momentum transfer leading to a noticeable shift in the asymmetry parameter β. The analysis performed demonstrates that this interaction between photoelectrons and Auger electrons is the main mechanism for angular-momentum transfer. The role of the interaction between the photoelectron and the residual ion in angular-momentum exchange is negligible. This situation is opposite to the PCI distorted energy distribution, which in the case of near-threshold ionization is governed by the photoelectron-ion interaction while the influence of fast Auger electrons is negligible.

The paper is organized as follows. In Sec. II, we develop the theory of angular-momentum transfer between Auger and photoelectrons. In Sec. III, the theory is extended for photoelectron-ion interaction. In Sec. IV, we apply the developed approach to the calculation of the asymmetry parameter β in the case of Ar $1s^2$ photoionization followed by single Auger decay. The atomic unit system $|e| = m_e = \hbar = 1$ is used throughout.

II. ANGULAR-MOMENTUM TRANSFER BETWEEN PHOTOELECTRONS AND AUGER ELECTRONS

In this section, we consider the mechanism of angular-momentum transfer between the outgoing photoelectron and Auger electron. Deep inner-shell photoionization followed by Auger decay of the atomic inner-shell vacancy is a two-step process that can be represented by the scheme

$$\begin{aligned}\gamma + A &\to e_{ph}(\varepsilon_0 + i\Gamma/2) + A^{+*} \\ &\to e_{ph}(\mathbf{p}_1) + e_A(\mathbf{p}_2) + A^{2+}. \end{aligned} \tag{1}$$

In the first step, the incident photon ionizes the ns^2 shell of the target atom resulting in the creation of a long-living metastable autoionizing state of the A^{+*} ion with autoionization width Γ and a photoelectron e_{ph} with complex energy $\varepsilon_0 + i\Gamma/2$ (ε_0 is the excess of photon energy above the threshold) moving in the field of the singly charged ion. In the second step, the long-living intermediate autoionizing state of the A^{+*} ion decays via Auger process resulting in the emission of a fast Auger electron e_A and the shake-off of the photoelectron motion by sudden change of the ion field from the potential of the A^{+*} ion to the field of the doubly charged ion A^{2+}. The amplitude $\mathcal{A}$ of the two-step process (1) is given by the product of the photoabsorption amplitude M_1 and the amplitude M_2 of the Auger decay of the autoionizing state A^{+*} and subsequent PCI processes [23,30]:

$$\mathcal{A} = M_1 \langle \Psi_{\mathbf{p}_1,\mathbf{p}_2}\, \Phi_{A^{2+}} | \hat{M}_2 | \Psi_{\varepsilon_0 + i\Gamma/2} \Phi_{A^{+*}} \rangle. \tag{2}$$

The photoabsorption amplitude M_1 slightly depends on the photon energy and below we will consider it a constant factor. In contrast, the second part of amplitude $\mathcal{A}$ has a strong resonant dependence on the energy of the outgoing photoelectron and describes the energy and angular-momentum transfer during PCI. Therefore, we consider below this part of the amplitude in details. In Eq. (2) $\Phi_{A^{+*}}$ is the wave function of the long-living intermediate autoionizing state and $\Psi_{\varepsilon_0 + i\Gamma/2}$ is the outgoing Coulomb partial wave of photoelectron e_{ph} in the intermediate state of process (1). This function describes the propagation of the photoelectron in the field of the A^{+*} ion. It can be obtained as a solution of the inhomogeneous

Schrödinger equation with complex energy $\varepsilon_0 + i\Gamma/2$ [23]. The real part of this energy ε_0 is the excess of photon energy above the inner-shell ionization threshold, while its imaginary part is determined by the autoionization width Γ of the inner-shell vacancy. We assume that the photoelectron is emitted from the deep ns^2 shell of target atom A and therefore has the angular momentum $l = 1$. The operator of the Auger decay is denoted here by $\hat{M}_2$. The wave function of the final state is given by the product of doubly charged ion wave function $\Phi_{A^{2+}}$ and the two-body wave function $\Psi_{\mathbf{p}_1,\mathbf{p}_2}$ of the photoelectrons and Auger electrons moving in the field of A^{2+} with momenta $\mathbf{p}_1$ and $\mathbf{p}_2$, respectively.

In our approach, the two-body wave function $\Psi_{\mathbf{p}_1,\mathbf{p}_2}$ is considered in the 3C approximation (the so-called BBK function) [31]. This approximation takes into account the interaction between the photoelectrons and Auger electrons, as well as their interaction with the ion field, and has the correct asymptotical behavior. Such a two-body function has the form

$$\Psi_{\mathbf{p}_1,\mathbf{p}_2}(\mathbf{r}_1,\mathbf{r}_2) = \Psi_{\mathbf{p}_1}(\mathbf{r}_1)\Psi_{\mathbf{p}_2}(\mathbf{r}_2)\phi(\mathbf{r}_1 - \mathbf{r}_2). \tag{3}$$

where $\Psi_{\mathbf{p}_{1,2}}(\mathbf{r}_{1,2})$ are the single-particle Coulomb functions of photoelectrons and Auger electrons moving in the field of the doubly charged ion and the function $\phi(\mathbf{r}_1 - \mathbf{r}_2)$ describes their relative motion. According to the 3C approximation [31] this function can be represented by the Coulomb wave $\Psi_{\mathbf{p}_1-\mathbf{p}_2}(\mathbf{r}_1 - \mathbf{r}_2)$ of the relative motion as

$$\phi(\mathbf{r}_1 - \mathbf{r}_2) = \Psi_{\mathbf{p}_1-\mathbf{p}_2}(\mathbf{r}_1 - \mathbf{r}_2)e^{-i(\mathbf{p}_1-\mathbf{p}_2)\cdot(\mathbf{r}_1-\mathbf{r}_2)}. \tag{4}$$

The following approximations are based on the fact that the Auger electron is very fast $p_2 \gg 1$. In this case, the wave function of the relative motion ϕ can be written in the eikonal approximation [32]

$$\phi(\mathbf{r}) = \exp\left(i\int_0^\infty \frac{e^2 dt}{|\mathbf{r} - \mathbf{v}t|}\right), \tag{5}$$

where $\mathbf{r} = \mathbf{r}_1 - \mathbf{r}_2$ and $\mathbf{v} = \mathbf{v}_1 - \mathbf{v}_2$ are the vectors of relative position and velocity of the photoelectrons and Auger electrons, respectively.

Evaluating amplitude $\mathcal{A}$, Eq. (2), one notes that the energy and angular distribution of the emitted photoelectrons are to a greater extent connected to the photoelectron wave functions in the Auger matrix element. It is important that the Auger decay operator $\hat{M}_2$ acts on the atomic and Auger electron coordinates, and does not effect directly the photoelectron coordinates. Evaluation the Auger decay amplitude M_2 is preformed on the atomic scale distances, $r_2 \sim 1$, while the overlap integral of the photoelectron wave functions is evaluated on the much larger spatial scale, $r_1 \gg 1$. Therefore, the relative electron coordinates $\mathbf{r} = \mathbf{r}_1 - \mathbf{r}_2$ in the amplitude $\mathcal{A}$ actually coincide with the photoelectron coordinates $\mathbf{r} \simeq \mathbf{r}_1$. This fact decouples the integrations over Auger and photoelectron coordinates and the amplitude $\mathcal{A}$ is reduced to the product of $M_{1,2}$ amplitudes and the overlap integral

$$\mathcal{A} = M_1\, M_2(\mathbf{p}_2, L, M)\, \langle \Psi_{\mathbf{p}_1}(\mathbf{r})\phi(\mathbf{r})|\Psi_{\varepsilon_0+i\Gamma/2}(\mathbf{r})\rangle. \tag{6}$$

Amplitude $M_2(\mathbf{p}_2, L, M)$ of the Auger decay depends on the angular momentum L and its projection M of the doubly charged ion in the final state. Apart from this, amplitude M_2 may depend on the direction of the Auger emission. However, it does not affect the angular distribution of the photoelectrons if the polarization of the resulting A^{2+} ion is not fixed. It can be demonstrated that during the evaluation of the cross section, after summation over all angular momentum states M of the A^{2+} ion, the angular dependence of $|M_2(\mathbf{p}_2)|^2$ vanishes for reasons of symmetry. Indeed, the Auger electron $e_A(\mathbf{p}_2)$ and the residual ion A^{2+} yield the same angular momentum L with opposite projections $\pm M$. The Auger amplitude depends on M and $\mathbf{p}_2$ as $M_2(\mathbf{p}_2, L, M) \propto Y_{LM}(\mathbf{p}_2)$. Thus, the sum of $|M_2(\mathbf{p}_2, L, M)|^2$ over M eliminates its dependence on the direction of $\mathbf{p}_2$ since $\sum_M |Y_{LM}(\mathbf{p}_2)|^2 = (2L+1)/4\pi$. So amplitudes M_2 and M_1 are considered from now on as numbers.

Evaluating the overlap integral in Eq. (6), we can simplify the eikonal form of function ϕ in Eq. (5). Namely, we have to take into account a large value for the Auger electron velocity, $v_2 \approx v \gg 1$. Hence, the exponential function in Eq. (5) can be expanded in a power series keeping only the first two terms. In the zeroth approximation $\phi(\mathbf{r}) = 1$, and amplitude $\mathcal{A}$ reduces to the well-known expression for the PCI amplitude [23,30]

$$\mathcal{A}^{(0)} = M_1\, M_2\, \langle \Psi_{\mathbf{p}_1}(\mathbf{r})|\Psi_{\varepsilon_0+i\Gamma/2}(\mathbf{r})\rangle. \tag{7}$$

This approximation neglects the interaction between the slow photoelectron and the fast Auger electron, the PCI distortion is caused by the shake-off process due to the Auger decay, and this approximation does not take into account the angular-momentum transfer. The outgoing photoelectron $e_{ph}(\mathbf{p}_1)$ carries the same angular momentum $l = 1$ as the intermediate photoelectron $e_{ph}(\varepsilon_0 + i\Gamma/2)$. The corresponding differential cross section reads as

$$\frac{d^2\sigma^{(0)}}{d\varepsilon d\Omega} = M\left|Y_{10}(\mathbf{n})\, R_{\varepsilon\,1,\varepsilon_0\,1}\right|^2 = \frac{3\,M}{4\,\pi}\left|R_{\varepsilon\,1,\varepsilon_0\,1}\right|^2 \sum_{k=0,2}\left(C^{k0}_{10\,10}\right)^2 P_k(\cos\theta), \tag{8}$$

where $C^{k0}_{10\,10}$ is the Clebsch-Gordan coefficient, M is the numerical factor containing the product of $|M_1 M_2|^2$ that depends smoothly on ε; $R_{\varepsilon\,l,\varepsilon_0\,1}$ is the overlap integral between the radial parts $\chi(r)$ of the photoelectron wave functions in the intermediate and final states:

$$R_{\varepsilon\,l,\varepsilon_0\,1} = \int_0^\infty \chi_{\varepsilon,\,l}(r)\chi^{(+)}_{\varepsilon_0+i\frac{\Gamma}{2},\,1}dr. \tag{9}$$

Functions χ are normalized to $2\pi\delta(\varepsilon' - \varepsilon)$ and have the standing wave asymptotic

$$\chi_{\varepsilon,l}(r) = \frac{2}{\sqrt{p_1}}\sin\left(p_1 r + \frac{2\,e^2}{p_1}\ln(2p_1 r) - \frac{\pi l}{2} + \delta_l\right) \tag{10}$$

for an outgoing photoelectron with energy $\varepsilon = p_1^2/2$ and asymptotic of the outgoing partial wave

$$\chi^{(+)}_{\varepsilon_0+i\frac{\Gamma}{2},1}(r) = \frac{1}{\sqrt{p_0}}\exp\left[i\left(p_0 r + \frac{e^2}{p_0}\ln(2p_0 r) - \frac{\pi}{2} + \delta_1\right)\right]. \tag{11}$$

for the intermediate photoelectron with the energy $\varepsilon_0 + i\Gamma/2 = p_0^2/2$.

Angular-momentum transfer can only be taken into account within the next approximation, which is equivalent to the first

Born approximation with respect to the Coulomb interaction between the photoelectrons and Auger electrons. The corresponding amplitude $\mathcal{A}^{(1)}$ is obtained by keeping in expression (6) the second term of the exponential function expansion for ϕ:

$$\mathcal{A}^{(1)} = -i\, M_1\, M_2\, \langle \Psi_{\mathbf{p}_1}(\mathbf{r})| \int_0^\infty \frac{e^2 dt}{|\mathbf{r}-\mathbf{v}t|} |\Psi_{\varepsilon_0 + i\Gamma/2}(\mathbf{r})\rangle. \quad (12)$$

Note that this approximation is equivalent to the approach that considers the distortion of the outgoing photoelectron wave function by the time-dependent external potential $V(t,\mathbf{r}) = e^2/|\mathbf{r}-\mathbf{v}t|$ provided by the Coulomb field of the classically moving fast Auger electron. Indeed, considering such an external potential as a small perturbation acting during a short time, one gets in first approximation exactly expression (12).

An evaluation of expression (12) is presented in the Appendix. It is shown that amplitudes $\mathcal{A}^{(0)}$ and $\mathcal{A}^{(1)}$ do not interfere in the cross section integrated over the Auger electron directions. Thus the cross section is given by the sum of zero-order contribution $\sigma^{(0)}$ (8) and contribution of the processes of the angular-momentum transfer. The latter one denoted here as $\sigma^{(2)}$ is represented as sum over all nonzero values of transferred angular momentum $l \neq 0$:

$$\begin{aligned}\frac{d^2\sigma^{(2)}}{d\varepsilon d\Omega} = {} & \frac{3M}{4\pi}\left(\frac{e^2}{v_2}\right)^2 \sum_k P_k(\cos\theta) C^{k0}_{10\,10} \\ & \times \sum_{l_1,l_2,l>0} e^{i(\delta_{l_1}-\delta_{l_2})} i^{l_2-l_1}(-1)^{l+l_1+l_2} \\ & \times R_{\varepsilon\, l_1,\varepsilon_0\, 1}\, R^*_{\varepsilon\, l_2,\varepsilon_0\, 1} \frac{(2l+1)}{l^2(l+1)^2}\sqrt{(2l_1+1)(2l_2+1)} \\ & \times \begin{Bmatrix} l & l_2 & 1 \\ k & 1 & l_1 \end{Bmatrix} C^{k0}_{l_1 0\, l_2 0} C^{l_1 0}_{l0\,10} C^{l_2 0}_{l0\,10}. \end{aligned} \quad (13)$$

Here, factor M has the same value as in Eq. (8), v_2 is the velocity of the Auger electron, $l_{1,2}$ denote the possible values of angular momenta in the final photoelectron state for given values of the transferred angular momentum l and the angular momentum $l = 1$ of the intermediate photoelectron state. The overlap integrals $R_{\varepsilon\, l_{1,2},\varepsilon_0\, 1}$ are defined by expression (9), the phases $\delta_{l_{1,2}}$ of the outgoing photoelectron wave functions are chosen according to Eq. (10). Note that according to the properties of the Clebsch-Gordan coefficient $C^{k0}_{10\,10}$, index k only runs through two values, $k = 1,2$, similarly to Eq. (8). This results from the averaging over all residual ion states and Auger electron emission directions.

III. ANGULAR-MOMENTUM TRANSFER FROM THE TARGET ION

In this section, we consider angular-momentum transfer between the residual ion and the emitted photoelectron. The interaction with the Auger electron considered in the previous section will be here neglected. There are various mechanisms such angular-momentum transfer, e.g., a rearrangement of the open outer shells of the A^{2+} ion or intershell electron correlation in the A^{2+} ion [25,29]. However, we are restricted here to processes that are not accompanied by a considerable energy transfer. Thus, rearrangement of the ionic outer shell, which changes the ionic energy by a value larger than the autoionization width, shifts the photoelectron energy far from the PCI resonance region. Therefore, we consider here neither rearrangement of outer shells nor intershell electron correlation. The latter is weak due to the large energy difference between the A^{2+} ion shells. Angular-momentum transfer without energy exchange may occur through photoelectron scattering on the asymmetrical part of the ionic potential. In the case of photoionization from a deep ns^2 shell of the spherical atom with closed shells considered here, an asymmetry of the mean-field potential appears only after Auger decay. At this time, the photoelectron is removed far from the target atom by a distance $r \sim v_1/\Gamma \gg 1$. At these distances, the higher multipoles of Coulomb interaction are rather small and hence the coupling between the angular momenta of the photoelectron and the residual ion is weak. In this case, the most effective mechanism for angular-momentum transfer is the precession of the angular momentum, which changes its projection while keeping its magnitude constant.

Such mechanism of angular-momentum transfer in single photoionization process of outer atomic shells had been described in Refs. [24,25]. Here, we apply this method to deep atomic shell photoionization followed by Auger decay. Our approach is based on the fact that after the fast Auger electron is gone, the system of an outgoing photoelectron and a residual ion $e_{ph} + A^{2+}$ conserves its total angular momentum L. The stationary state of such a system with the total angular momentum L and its projection M is given by the superposition

$$|\Psi_{LM}\rangle = \sum_{m,m_a} C^{LM}_{lm\, L_a m_a} \left|\Phi_{L_a m_a} \Psi_{lm}\right\rangle, \quad (14)$$

where $\Phi_{L_a m_a}$ denotes the wave function of the A^{2+} ion with angular momentum L_a and its projection m_a, Ψ_{lm} is the photoelectron partial wave with angular momentum l and its projection m. Since we neglect here the direct interaction between the photoelectron and the Auger electron, $\phi = 1$ in Eq. (3), the angular momentum of the photoelectron does not change with the Auger decay, i. e., $l = 1, m = 0$ in the case of ns^2 photoionization. During precession, the angular-momentum magnitude conserves, $l = 1$, while its projection m varies. Therefore, the final-state wave function of the system $e_{ph}(\mathbf{p}_1) + A^{2+}(L_a, m_f)$ is written as:

$$\begin{aligned} & |\Phi_{L_a m_f} \Psi_{\mathbf{p}_1}\rangle \\ & = \frac{2\pi}{\sqrt{p_1}} \sum_{mLM} C^{LM}_{lm\, L_a m_f} Y^*_{lm}(\mathbf{p}_1) e^{-i\left(\delta(L_a,L,l) - \frac{\pi l}{2}\right)} |\Psi_{LM}\rangle, \end{aligned} \quad (15)$$

where $\delta(L_a, L, l)$ is the phase shift of the photoelectron wave. Here, we use the partial wave expansion for $\Psi_{\mathbf{p}_1}$, Eq. (A1). Now, we can substitute the final-state wave function (15) into Eq. (2) for amplitude $\mathcal{A}$. The integration over the coordinates of operator $\hat{M}_2$ is similar to the one used in Eq. (6) and

leads to

$$\mathcal{A}(\mathbf{p}_1\mathbf{p}_2 L_a m_f) = \frac{2\pi\, M_1}{\sqrt{p_1}} \sum_{m m_i L M} C^{LM}_{lm\, L_a m_f} Y_{lm}(\mathbf{p}_1) e^{i\left(\delta(L_a,L,l)-\frac{\pi l}{2}\right)} \times M_2(\mathbf{p}_2, L_a, m_i) C^{LM}_{10\, L_a m_i} R(L_a, L, \varepsilon\, l, \varepsilon_0\, 1), \quad (16)$$

where m_i is the angular-momentum projection of the A^{2+} ion just after the Auger decay event and we introduce the notation

$$R(L_a, L, \varepsilon\, l, \varepsilon_0\, 1) = \int_0^\infty \chi^{L_a,L}_{\varepsilon,l}(r)\, \chi^{(+)}_{\varepsilon_0 + i\frac{\Gamma}{2},1}(r)\, dr \quad (17)$$

for the overlap integral of the radial parts of the photoelectron wave functions before and after the Auger decay. It differs from the similar integral (9) by the dependence of the $\chi^{L_a,L}_{\varepsilon,l}(r)$ function on the angular momenta L, L_a.

The Auger decay amplitude $M_2(\mathbf{p}_2, L_a, m_i)$ depends on the direction of the Auger electron emission as $Y^*_{L_a m_i}(\mathbf{p}_2)$. With the averaging of the cross section over the direction of an Auger electron emission the dependence of $|M_2(\mathbf{p}_2, L_a, m_i)|^2$ on $\mathbf{n}_{p_2}$ vanishes and terms with different values m_i do not interfere due to the orthogonality of the spherical harmonics.

The cross section is given by the square of the modulus of amplitude (16). Additionally, we have to sum the cross section over the projections m_f of the final ion states and to integrate over the Auger electron momenta, taking into account energy conservation. The product of the photoelectron spherical harmonics is written through Legendre polynomials $P_k(\cos\theta)$ in Eq. (A8), whereas the sums over the angular-momentum projections m, m_f and m_i, M are carried out with the help of Eq. (A9). The resulting cross section is given by the sum of partial cross sections corresponding to different values of the residual ion angular momentum L_a:

$$\frac{d^2\sigma}{d\varepsilon d\Omega} = \sum_{L_a} \frac{d^2\sigma^{(L_a)}}{d\varepsilon d\Omega} = \sum_{L_a} M_a \frac{(2l+1)}{4\pi\,(2L_a+1)} \times \sum_{k L L'} P_k(\cos\theta)(2L+1)(2L'+1)\left(C^{k0}_{l0l0}\right)^2 \times \begin{Bmatrix} l & l & k \\ L & L' & L_a \end{Bmatrix}^2 R(L_a, L, \varepsilon\, l, \varepsilon_0\, 1) \times R^*(L_a, L', \varepsilon\, l, \varepsilon_0\, 1) e^{i\delta(L_a,L,l) - i\delta(L_a,L',l)}, \quad (18)$$

where $l = 1$, M_a are the numerical factors proportional to $M_a \propto \int |M_2(\mathbf{p}_2, L_a, m_i)|^2 d\mathbf{n}_{p_2}$ and their sum $\sum_a M_a = M$ equals to the same constant as in Eq. (8).

Note that the angular-momentum transfer mechanism described is based on the dependence of phases $\delta(L_a, L, l)$ and overlap integrals $R(L_a, L, \varepsilon\, l, \varepsilon_0\, 1)$ on the total angular momentum L. If we neglect these dependencies, Eq. (18) immediately reduces to Eq. (8). The overlap integrals $R(L_a, L, \varepsilon\, l, \varepsilon_0\, 1)$ have resonance maximum at $\varepsilon \simeq \varepsilon_0$. The main contribution comes from the distances $r \sim v_1/\Gamma \gg 1$ corresponding to the position of photoelectron at the moment of the Auger decay. At these distances, the coupling between angular momenta of e_{ph} and A^{2+} is weak and the angular-momentum transfer due to angular-momentum precession is suppressed, as can be seen in Eq. (18).

Let us consider the case of an extremely long-living autoionizing state, $\Gamma^{-1} \gg 1$. The main contribution to the overlap integral (17) comes from the overlapping of the incoming part of the standing partial wave $\chi^{L_a,L}_{\varepsilon,l}(r)$ with the outgoing partial wave $\chi^{(+)}_{\varepsilon_0 + i\frac{\Gamma}{2},1}(r)$ of the photoelectron on a large radius scale where the asymptotic expressions (10), (11) are valid. Therefore, $R(L_a, L, \varepsilon\, l, \varepsilon_0\, 1) \propto \exp[-i\delta(L_a, L, l)]$ and the corresponding phase factor in Eq. (18) cancels out. Hence, the dependence on L in Eq. (18) vanishes and it reduces to Eq. (8). It means that the photoionization process accompanied by angular-momentum transfer caused by the precession of angular momentum does not contribute to the leading resonance part of the photoionization cross section in Eq. (18). Angular-momentum transfer between e_{ph} and A^{2+} manifests itself only in the nonresonance terms that are smaller than the leading resonance term by the parameter $(\Gamma/8\varepsilon_0)^2 \ll 1$. This conclusion does not concern the precession mechanism of angular-momentum transfer solely but is true for all processes of angular-momentum transfer between the target ion and photoelectron. Indeed, this type of angular-momentum transfer is caused by the asymmetrical part of the ionic potential that appears due to the Auger decay when the photoelectron is located far from the ion, which in turn significantly reduces the efficiency of such an angular-momentum transfer. According to the arguments outlined above the influence of any processes of angular-momentum transfer between e_{ph} and A^{2+} on the photoelectron emission cross section will be suppressed in the region of the PCI resonance by a small factor $(\Gamma/8\varepsilon_0)^2$.

IV. RESULTS AND DISCUSSION

The differential cross sections obtained in Secs. II [Eqs. (8), (13)] and III [Eq. (18)] lead to similar angular distribution, which can be written as the sum of the two first Legendre polynomials $P_k(\cos\theta), k = 0, 2$:

$$\frac{d^2\sigma}{d\varepsilon d\Omega} = \frac{\sigma}{4\pi}\left[1 + \beta\, P_2(\cos\theta)\right], \quad (19)$$

where σ is the total photoionization cross section and θ is the angle between the direction of photoelectron emission and the photon polarization vector (we consider here the case of linearly polarized photons). It is worth noting that in such angular distribution pattern we fix neither the direction of the Auger electron emission nor the polarization of the residual ion. Cross section (19) has been integrated over $\mathbf{p}_2$ and summed over all states of the residual ion. The only predominant direction is the photon polarization vector, so the photoemission angular distribution is characterized by a single parameter, β, known as an anisotropy parameter. In the case of the zero angular-momentum transfer, when the emitted photoelectron carries the angular momentum of the photon, $l = 1, m = 0$, the photoionization cross section is given by Eq. (19) with $\beta = 2$ [25]. Therefore, deviation of β from this value, $\Delta\beta = 2 - \beta$, indicates the occurrence of angular-momentum transfer.

As an example, we will apply the theory developed above to the photoionization of the $1s^2$ shell of argon. The decay of the inner $1s$ vacancy shows a rather complicated dynamics [7,33]. The main channel leading to the creation of the Ar^{2+}

ions includes the radiative decay of the inner vacancy $1s^{-1} \to 2p^{-1} + \gamma$ followed by the Auger decay $2p^{-1} \to 3p^{-2} + e_A$ with emission of fast Auger electron e_A ($E_A \simeq 200$ eV) [33]. The widths of the $1s$ and $2p$ vacancies are equal to $\Gamma_{1s} = 690\,\text{meV}$ [34] and $\Gamma_{2p} = 118\,\text{meV}$ [35], respectively. This channel is in competition with the weaker direct Auger decay of the inner $1s$ vacancy $1s^{-1} \to 3p^{-2} + e_A$ with the Auger electron energy $E_A \simeq 3150$ eV [33].

First, we examine the angular-momentum transfer between the photoelectron and the Auger electron, and determine the corresponding anisotropy parameter β according to the approach developed in Sec. II. The main channel for the $1s$ vacancy decay of Ar^{+*} is a cascade process, as seen above, instead of a simpler direct Auger decay considered in our theory. Nevertheless, the results of Sec. II, in Eqs. (8) and (13), can be applied to the Ar $1s$ photoionization. Indeed, the first radiative decay $1s^{-1} \to 2p^{-1} + \gamma$ of the inner vacancy occurs after long delay $\tau_{1s} = 1/\Gamma_{1s}$ when the photoelectron has already moved away from the ion. Thus, the radiative decay will add some weak higher multipoles to the Coulomb interaction of Ar^{+*} and e_{ph}, which can be neglected here. The ionic mean field undergoes a considerable change only at the moment of the Auger decay. Therefore, considering angular-momentum transfer between photoelectrons and Auger electrons, we can treat for simplicity the two-step decay process as a single Auger decay with the effective decay time $\tau_{\text{eff}} = \tau_{1s} + \tau_{2p}$ and corresponding effective autoionization width $\Gamma_{\text{eff}} = \Gamma_{1s}\,\Gamma_{2p}/(\Gamma_{1s} + \Gamma_{2p})$ [7]. In our case, it gives $\Gamma_{\text{eff}} = 101\,\text{meV}$.

We have calculated the photoionization cross sections as a sum of zeroth, $\sigma^{(0)}$, and first Born, $\sigma^{(2)}$, approximation contributions with respect to the e_{ph}-e_A interaction according to Eqs. (8) and (13) for photon energy excess above the $1s$ threshold $\varepsilon_0 = 2\,\text{eV}$. This energy is smaller by two orders of magnitude than the Auger electron energy 200 eV [33], assuring the applicability of the approximations employed.

The outgoing partial wave function $\chi^{(+)}_{\varepsilon_0 + i\frac{\Gamma}{2},1}(r)$ of the intermediate electronic state in the overlap integrals Eq. (9) has been calculated in the Hartree-Fock (HF) approximation as a solution of the inhomogeneous Schrödinger equation by the method described in Refs. [23,36]. The wave functions $\chi_{\varepsilon,l_{1,2}}(r)$ of the photoelectron moving in the field of the final ionic state Ar^{2+} with two $3p$ holes were also calculated in the HF approximation. In our calculations, we take into account 12 partial photoelectron waves with angular momenta $0 \leqslant l_{1,2} \leqslant 11$, although convergence of the results was achieved at $l_{1,2} \simeq 7$.

The results obtained are presented in Fig. 1(a) as a function of photoelectron energy. The solid red and blue dashed lines show the total photoionization cross sections $\sigma^{(0)}$ and $\sigma^{(2)}$ calculated in the zeroth, Eq. (8), and the first Born, Eq. (13), approximations, respectively. We also plot the partial contributions from transferred angular momentum $l = 1$ and $l = 10$, as olive dotted and magenta dash-dotted lines respectively. All curves in Fig. 1(a) show the resonance behavior that results from the properties of the overlap integrals $R_{\varepsilon\, l_{1,2},\varepsilon_0\, 1}$ (9). The overlapping between the radial wave functions of the final, $\chi_{\varepsilon,l}(r)$, and the intermediate, $\chi^{(+)}_{\varepsilon_0 + i\frac{\Gamma}{2},1}(r)$, photoelectron states is maximal if their momenta coincide.

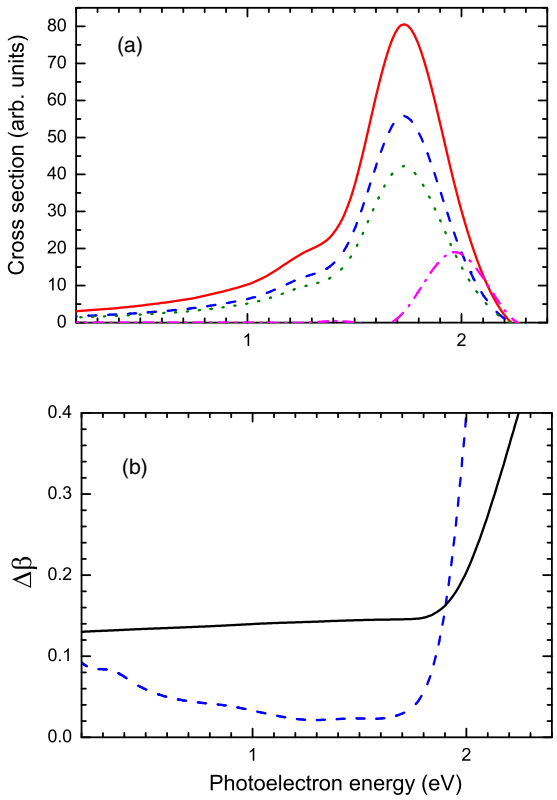

FIG. 1. (a) The total photoionization cross sections as a function of photoelectron energy. The solid red line shows the cross section $\sigma^{(0)}$, Eq. (8), calculated in zero approximation, the dashed blue line presents the cross section $\sigma^{(2)} \times 10$, Eq. (13), calculated in the first Born approximation, the olive dotted line represents the partial contributions to $\sigma^{(2)}$ from transferred angular momentum $l = 1$ multiplied by 10 and the magenta dash-dotted line shows the partial contributions to $\sigma^{(2)}$ from transferred angular momentum $l = 10$ multiplied by 10^3. (b) The alteration of the parameter β as a function of photoelectron energy. Black solid line shows $\Delta\beta$ calculated according to Eqs. (8), (13) for the e_{ph}-e_A interaction. Blue dashed line shows $\Delta\beta \times 10^3$ calculated according to Eq. (18) for the e_{ph}-Ar^{2+} interaction.

Physically it means that, at the time of the Auger decay, the photoelectron momentum does not change. Consequently, neglecting Coulomb interaction, the resonance condition is $\varepsilon \simeq \varepsilon_0$. PCI between the photoelectron and the ion affects this condition, resulting in the well-known distortion of the cross section shapes [19]. Attraction of the outgoing photoelectron by the Coulomb field of the double-charged ion decreases its kinetic energy by a factor of two compared to the single-charged ion field. This effect shifts the photoemission energy distribution towards the negative energy difference $\varepsilon - \varepsilon_0 < 0$. Larger energy difference corresponds to smaller electron-ion distances at which the Auger decay takes place and vice versa. Larger distances lead to larger values of the overlap integral forming the left shoulder of the PCI peak. At positive energy difference $\varepsilon - \varepsilon_0 > 0$, the resonance condition for maximal wave functions overlap can not be fulfilled at any distances. It leads to the sharp cutoff of PCI peak above the resonance.

Angular-momentum transfer also leads to the energy distortion due to same mechanism as for the Coulomb interaction described above, but the direction of the distortion is opposite [26]. Indeed, angular-momentum transfer increases the photoelectron angular momentum and corresponding rotational energy. The increase of outgoing photoelectron energy shifts in turn the PCI peak position in the positive direction. This effect can be seen in the behavior of the partial contributions of $\sigma^{(2)}$ presented in the Fig. 1(a). The energy shift of the partial contribution of the transferred angular momentum $l = 1$ (olive dotted line) is practically zero. This happens because one value of the possible angular momentum of the outgoing photoelectron $l_{1,2} = l - 1 = 0$ is smaller than the angular momentum of the intermediate state while another value $l_{1,2} = l + 1 = 2$ is larger. For higher transferred angular momenta the outgoing photoelectron angular momenta $l_{1,2} = l \pm 1$ become larger, which results in a sizable energy shift. For illustration, we show in Fig. 1(a) by the magenta dot-dashed line the partial contribution of the transferred angular momentum $l = 10$ when the outgoing photoelectron has the angular momenta $l_{1,2} = 9, 11$.

Note that the partial contributions decrease rapidly with increasing angular-momentum transfer. As can be seen in Fig. 1(a) the partial contribution of the transferred angular momentum $l = 10$ is smaller by two orders of magnitude than the contribution of $l = 1$. The total contribution of the angular-momentum transfer process $\sigma^{(2)}$ is smaller by an order of magnitude than $\sigma^{(0)}$. Nevertheless, its contribution is sufficient to introduce a noticeable change in the parameter β as shown in Fig. 1(b) by a black solid line. Within the PCI resonance region, its alteration with respect to the zeroth approximation value $\beta = 2$ amounts to $\Delta\beta \simeq 0.15$. Above the resonance region where the cross section $\sigma^{(0)}$ decreases sharply $\Delta\beta$ increases rapidly because of the increasing influence of the higher transferred angular momenta. The latter is explained by two features described above: the sharp cross-section cutoff above the PCI peak and positive energy shift of the PCI peak for higher transferred angular momenta.

For comparison, we also show in Fig. 1(b) the effect of angular-momentum transfer between e_{ph} and Ar^{2+}. The blue dashed line shows the energy dependence of $\Delta\beta$ multiplied by 10^3, β is calculated according to Eq. (18). For the calculation, we chose the direct Auger decay channel of the inner vacancy: $1s^{-1} \to 3p^{-2} + e_A$. It is not the main decay channel but in this case the intermediate Ar^+ ion state before the Auger decay is spherically symmetric and it is just the case, which has been considered in Sec. III. The total angular momentum of the Ar^{2+} outer shell ($3p^4$) can have three different values $L_a = 0, 1, 2$. The photoelectron final-state wave functions $\chi_{\varepsilon,1}^{L_a,L}(r)$ are calculated in the HF approximation also. However, in this case, we have taken into account the dependence of these functions on the angular momentum L_a of the ion and on the total angular momentum L of the system $e_{ph} + Ar^{2+}$.

Figure 1(b) shows that angular-momentum transfer between e_{ph} and e_A is much more effective than between e_{ph} and Ar^{2+}. The change in β parameter, $\Delta\beta$, due to the first mechanism is by four orders of magnitude stronger than the second one. There are several reasons why angular-momentum transfer between e_{ph} and Ar^{2+} is weak. One reason has been already discussed above. It is connected to the specific feature of a photoionization process accompanied by PCI, namely the long delay between the s-shell photoionization and the symmetry breaking of the target ion after Auger decay. Consequently, this mechanism of angular-momentum transfer starts to work when the photoelectron is already located far away from the ion $r \sim v_1/\Gamma \gg 1$. For the considered PCI process this estimation gives $r \sim 100$. Therefore, this angular-momentum transfer is suppressed for the PCI resonance process and $\Delta\beta$ should tend to zero while photoelectron energy approaches the PCI resonance. Fig. 1(b) confirms this conclusion. Indeed, $\Delta\beta$ calculated for this mechanism demonstrates the antiresonance behavior. Such a behavior was explained in the previous section where it has been demonstrated that the different phase factors cancel each other in the dominant resonance term of Eq. (18) and, hence, the resonance term does not contribute to $\Delta\beta$.

Moreover, even apart from this effect, $\Delta\beta$ caused by e_{ph}-Ar^{2+} interaction is rather small. Indeed, our numerical calculations show that the typical variation of phase shifts $\delta(L_a, L, l)$ under the variation of L is small, $\Delta\delta \sim 10^{-1}$. According to the Eq. (18) $\Delta\beta \propto (\Delta\delta)^2$ and therefore the shift of asymmetry parameter β should not exceed one percent even if we neglect the antiresonance effect discussed above. This conclusion is confirmed also by our numerical simulations. This estimation can be considered as the upper limit for $\Delta\beta$ caused by e_{ph}-Ar^{2+} interaction in an arbitrary case of inner-shell photoionization, including the photoionization of the nonspherical atoms. In the latter case, precession of the e_{ph} angular momentum starts immediately after the photoionization, but nevertheless its contribution to $\Delta\beta$ is by an order of magnitude smaller than due to the e_{ph}-e_A interaction.

We have also calculated the contribution to $\Delta\beta$ due to elastic photoelectron scattering on the anisotropic ionic potential, resulting in a variation of the photoelectron angular momentum, $l \neq 1$. We used the first Born approximation to calculate the corresponding cross sections and their contribution to the angular-momentum transfer between e_{ph} and Ar^{2+}. The result was even smaller than for the precession mechanism. So we conclude that the e_{ph}-Ar^{2+} interaction does not practically influence the angular-momentum transfer.

In the present paper, we did not consider the influence of the relativistic effects on the angular distribution of the photoelectron. The spin-orbit interaction as well as nondipole terms of the electron-photon interaction may affect the angular distribution of the emitted photoelectrons. In the case of the photoionization of Ar, we estimate their effect on β to be less than one percent, i.e., much smaller than the effect of the e_{ph}-e_A interaction. The latter seems to largely dominate the angular-momentum transfer in the photoionization processes considered.

It should be noted that the roles played by the interaction between the photoelectron and the ion field and between the photoelectron and the Auger electron are quite different in the energy region close to the inner-shell ionization threshold. The e_{ph}-Ar^{n+} interaction mainly affects the energy distribution of the emitted photoelectrons; the effect of the e_{ph}-e_A interaction is negligible if the photoelectron is much slower than the Auger electron. In contrast to that, the e_{ph}-e_A interaction is responsible for the angular-momentum transfer and is

rather effective in the distortion of the photoelectron angular distribution even if the Auger electron is much faster than the photoelectron.

Concerning the possibility of an experimental observation of the angular-momentum transfer it is worth to note that the predicted shift of the anisotropy parameter β does not exceed ten percent of its nonshifted value at the zero angular-momentum transfer. This is why the presence of slow occasional electrons in the PCI resonance region may noticeably decrease the accuracy of the $\Delta\beta$ measurements. Therefore, the experimental method should assure that the only photoelectrons emitted in the selected resonance PCI process (1) are detected.

V. CONCLUSION

The angular distribution of the photoemission from deep atomic ns^2 inner shells was investigated. A theoretical approach to PCI in photoionization processes taking into account angular-momentum transfer between the emitted photoelectron, Auger electron, and target ion was developed. It is demonstrated that the main contribution to angular-momentum transfer changing noticeably the photoemission angular distribution comes from the interaction between the photoelectrons and the Auger electrons. The developed theory has been applied to the photoionization of the $1s^2$ shell of Ar. We report a 0.15 decrease of the anisotropy parameter β in the region of the PCI resonance caused by angular-momentum transfer between the photoelectrons and the Auger electron. It is also demonstrated that the effect of all others mechanisms of angular-momentum transfer is smaller by several orders of magnitude.

APPENDIX: EVALUATION OF CROSS SECTION IN THE FIRST BORN APPROXIMATION

To evaluate the amplitude (12), we use the partial wave expansion for the outgoing photoelectron wave function

$$\Psi_{\mathbf{p}_1}(\mathbf{r}) = 2\pi i \sum_{lm} \frac{e^{i\left(\frac{\pi l}{2}-\delta_l\right)}}{\sqrt{p_1}\, r} Y^*_{lm}(\mathbf{p}_1)\chi_{\varepsilon,l}(r)Y_{lm}(\mathbf{n}), \tag{A1}$$

the multipole expansion for the Coulomb potential

$$\frac{e^2}{|\mathbf{r}_1-\mathbf{r}_2|} = 4\pi e^2 \sum_{lm} \frac{r_<^l}{r_>^{l+1}} \frac{Y_{lm}(\mathbf{n}_1)Y^*_{lm}(\mathbf{n}_2)}{2l+1}, \tag{A2}$$

and select the radial part in the intermediate photoelectron wave function:

$$\Psi_{\varepsilon_0+i\Gamma/2}(\mathbf{r}) = \frac{\chi^{(+)}_{\varepsilon_0+i\Gamma/2,1}(r)}{r} Y_{1\,0}(\mathbf{n}). \tag{A3}$$

The direct integration over t in Eq. (12) using Eq. (A2) leads to

$$\int_0^\infty \frac{e^2}{|\mathbf{r}-\mathbf{v}t|}\, dt = \frac{4\pi e^2}{v} \sum_{l>0,m} \frac{Y_{lm}(\mathbf{n})Y^*_{lm}(\mathbf{v})}{(l+1)l}. \tag{A4}$$

Here we omit the monopole term since it does not lead to angular-momentum transfer.

Eventually, we obtain the following multipole expansion for amplitude $\mathcal{A}^{(1)}$

$$\begin{aligned}\mathcal{A}^{(1)} = -2\pi i\, M_1\, M_2 \left(\frac{4\pi e^2}{v_2}\right) \sum_{l_1,m_1,l>0,m} & \frac{e^{-i\left(\frac{\pi l}{2}-\delta_l\right)}}{\sqrt{p_1}} Y_{l_1m_1}(\mathbf{p}_1) \\ \times & \frac{\langle Y_{l_1m_1}(\mathbf{n}')|Y_{lm}(\mathbf{n}')|Y_{1\,0}(\mathbf{n}')\rangle Y^*_{lm}(\mathbf{v}_2)}{l(l+1)} \\ \times & \int_0^\infty \chi_{\varepsilon,l}(r)\chi^{(+)}_{\varepsilon_0+i\frac{\Gamma}{2},1}(r)dr,\end{aligned} \tag{A5}$$

where we replace the relative velocity vector $\mathbf{v}$ by the Auger electron velocity $\mathbf{v}_2$ because $v_1 \ll v_2 \simeq v$. The spherical functions matrix element is reduced to [37]

$$\langle Y_{l_1m_1}(\mathbf{n}')|Y_{lm}(\mathbf{n}')|Y_{1\,0}(\mathbf{n}')\rangle = \sqrt{\frac{3(2l+1)}{4\pi(2l_1+1)}} C^{l_1m_1}_{lm10} C^{l_1 0}_{l010}. \tag{A6}$$

The angular-momentum transfer amplitude $\mathcal{A}^{(1)}$ given by Eq. (A5) leads to additional contribution to the cross section. The latter is determined by the square of the modulus of the amplitudes sum $|\mathcal{A}^{(0)}+\mathcal{A}^{(1)}|^2$. Note that the zeroth-order amplitude $\mathcal{A}^{(0)}$ (7) does not depend on the emission direction of the Auger electron while the first-order amplitude $\mathcal{A}^{(1)}$ does via spherical harmonics $Y^*_{lm}(\mathbf{v}_2)$ [see Eq. (A5)]. The interference terms between $\mathcal{A}^{(0)}$ and $\mathcal{A}^{(1)}$ amplitudes in the cross section vanish due to the averaging over all directions of the Auger electron velocity $\mathbf{v}_2$. Moreover, all contributions corresponding to different values of transferred angular momentum l also do not interfere. Consequently, the process of angular-momentum transfer gives an additional separate contribution to the cross section, which is represented as a sum over the transferred angular momentum $l \neq 0$:

$$\begin{aligned}\frac{d^2\sigma^{(2)}}{d\varepsilon d\Omega} = M\left(\frac{e^2}{v_2}\right)^2 & \\ \times \sum_{l_1,l_2,l>0,m} & \frac{3(2l+1)e^{i(\delta_{l_1}-\delta_{l_2})}i^{l_2-l_1}}{\sqrt{(2l_1+1)(2l_2+1)}} Y_{l_1m}(\mathbf{p}_1)Y^*_{l_2m}(\mathbf{p}_1) \\ \times & \frac{R_{\varepsilon\, l_1,\varepsilon_0\, 1}R^*_{\varepsilon\, l_2,\varepsilon_0\, 1}}{l^2(l+1)^2} C^{l_1m}_{lm10}C^{l_10}_{l010}C^{l_2m}_{lm10}C^{l_20}_{l010},\end{aligned} \tag{A7}$$

where we use the notation (9) for overlap integrals and factor M is the same as in Eq. (8).

The product of spherical harmonics can be represented through the Legendre polynomials $P_k(\cos\theta)$ as [37]

$$\begin{aligned}Y_{l_1m}(\mathbf{n})Y^*_{l_2m}(\mathbf{n}) = (-1)^m & \frac{\sqrt{(2l_1+1)(2l_2+1)}}{4\pi} \\ \times & \sum_k C^{k0}_{l_1m\,l_2-m}C^{k0}_{l_10\,l_20}P_k(\cos\theta),\end{aligned} \tag{A8}$$

after that the sum over m in Eq. (A7) equals to [37]

$$\begin{aligned}\sum_m (-1)^m C^{k0}_{l_1m\,l_2-m}C^{l_1m}_{lm10}C^{l_2m}_{lm10} & \\ = (-1)^{l+l_1+l_2}\sqrt{(2l_1+1)(2l_2+1)}\, C^{k0}_{10\,10} \begin{Bmatrix} l & l_2 & 1 \\ k & 1 & l_1 \end{Bmatrix}.\end{aligned} \tag{A9}$$

With the help of Eqs. (A8) and (A9) we finally obtain

$$\frac{d^2\sigma^{(2)}}{d\varepsilon d\Omega} = \frac{3M}{4\pi}\left(\frac{e^2}{v_2}\right)^2 \sum_k P_k(\cos\theta) C^{k0}_{10\,10} \sum_{l_1,l_2,l>0} e^{i(\delta_{l_1}-\delta_{l_2})} i^{l_2-l_1}(-1)^{l+l_1+l_2} R_{\varepsilon\, l_1,\varepsilon_0\, 1} R^*_{\varepsilon\, l_2,\,\varepsilon_0\, 1} \frac{(2l+1)}{l^2(l+1)^2}$$
$$\times \sqrt{(2l_1+1)(2l_2+1)} \begin{Bmatrix} l & l_2 & 1 \\ k & 1 & l_1 \end{Bmatrix} C^{k0}_{l_1 0\, l_2 0} C^{l_1 0}_{l 0 1 0} C^{l_2 0}_{l 0 1 0}. \tag{A10}$$

[1] M. Yu. Kuchiev and S. A. Sheinerman, Sov. Phys. Usp. **32**, 569 (1989).
[2] V. Schmidt, Rep. Prog. Phys. **55**, 1483 (1992).
[3] A. K. Kazansky and N. M. Kabachnik, Phys. Rev. A **72**, 052714 (2005).
[4] A. K. Kazansky and N. M. Kabachnik, J. Phys. B: At. Mol. Opt. Phys. **39**, L53 (2006).
[5] F. Penent, S. Sheinerman, L. Andric *et al.*, J. Phys. B: At. Mol. Opt. Phys. **41**, 045002 (2008).
[6] L. Gerchikov and S. Sheinerman, Phys. Rev. A **84**, 022503 (2011).
[7] R. Guillemin, S. Sheinerman, C. Bomme, L. Journel, T. Marin, T. Marchenko, R. K. Kushawaha, N. Trcera, M. N. Piancastelli, and M. Simon, Phys. Rev. Lett. **109**, 013001 (2012).
[8] S. Sheinerman, P. Linusson, J. H. D. Eland, L. Hedin, E. Andersson, J. E. Rubensson, L. Karlsson, and R. Feifel, Phys. Rev. A **86**, 022515 (2012).
[9] J. Palaudoux, S. Sheinerman, J. Soronen *et al.*, Phys. Rev. A **92**, 012510 (2015).
[10] R. Guillemin, S. Sheinerman, R. Püttner, T. Marchenko, G. Goldsztejn, L. Journel, R. K. Kushawaha, D. Ceolin, M. N. Piancastelli, and M. Simon, Phys. Rev. A **92**, 012503 (2015).
[11] P. van der Straten, R. Morgenstern, and A. Niehaus, Z. Phys. D **8**, 35 (1988).
[12] M. Yu. Kuchiev and S. A. Sheinerman, Sov. Phys. JETP **63**, 986 (1986).
[13] M. Yu. Kuchiev and S. A. Sheinerman, J. Phys. B: At. Mol. Opt. Phys. **21**, 2027 (1988).
[14] M. Yu. Kuchiev and S. A. Sheinerman, J. Phys. B: At. Mol. Opt. Phys. **27**, 2943 (1994).
[15] A. L. Landers, F. Robicheaux, T. Jahnke, M. Schoffler, T. Osipov, J. Titze, S. Y. Lee, H. Adaniya, M. Hertlein, P. Ranitovic, I. Bocharova, D. Akoury, A. Bhandary, T. Weber, M. H. Prior, C. L. Cocke, R. Dorner, and A. Belkacem, Phys. Rev. Lett. **102**, 223001 (2009).
[16] F. Robicheaux, M. P. Jones, M. Schoffler *et al.*, J. Phys. B: At. Mol. Opt. Phys. **45**, 175001 (2012).
[17] Qianxia Wang, S. Sheinerman, and F. Robicheaux, J. Phys. B: At. Mol. Opt. Phys. **47**, 215003 (2014).
[18] G. C. King, F. H. Read, and R. C. Bradford, J. Phys. B: At. Mol. Phys. **8**, 2210 (1975).
[19] A. Niehaus, J. Phys. B: At. Mol. Phys. **10**, 1845 (1977).
[20] M. Ya. Amus'ya, M. Yu. Kuchiev, and S. A. Sheinerman, Sov. Phys. JETP **49**, 238 (1979).
[21] K. Helenelund, S. Hedman, L. Asplund, U. Gelius, and K. Siegbahn, Phys. Scr. **27**, 245 (1983).
[22] G. B. Armen, T. Aberg, J. C. Levin, B. Crasemann, M. H. Chen, G. E. Ice, and G. S. Brown, Phys. Rev. Lett. **54**, 1142 (1985).
[23] M. Yu. Kuchiev and S. A. Sheinerman, J. Phys. B: At. Mol. Phys. **18**, L551 (1985).
[24] D. Dill, A. F. Starace, and S. T. Manson, Phys. Rev. A **11**, 1596 (1975).
[25] S. T. Manson and A. F. Starace, Rev. Mod. Phys. **54**, 389 (1982).
[26] A. Niehaus and C. J. Zwakhals, J. Phys. B: At. Mol. Phys. **16**, L135 (1983).
[27] M. K. Bahl, R. L. Watson, and K. J. Irgollic, Phys. Rev. Lett. **42**, 165 (1979).
[28] S. Hedman, K. Helenelund, L. Asplund, U. Gelius, and K. Siegbahn, J. Phys. B: At. Mol. Phys. **15**, L799 (1982).
[29] M. Ya. Amusia, *Atomic Photoeffect* (Plenum Press, New York, 1990).
[30] S. A. Sheinerman, J. Phys. B: At. Mol. Opt. Phys. **36**, 4435 (2003).
[31] M. Brauner, J. S. Briggs, and H. Klar, J. Phys. B: At. Mol. Opt. Phys. **22**, 2265 (1989).
[32] L. D. Landau and E. M. Lifshitz, *Quantum Mechanics*, 3rd ed. (Butterworth-Heinemann, Amsterdam, 1977), Chap. VI.
[33] U. Alkemper, J. Doppelfeld, and F. von Busch, Phys. Rev. A **56**, 2741 (1997).
[34] M. O. Krause, J. Phys. Chem. Ref. Data **8**, 307 (1979).
[35] M. Jurvansuu, A. Kivimäki, and S. Aksela, Phys. Rev. A **64**, 012502 (2001).
[36] M. Yu. Kuchiev and S. A. Sheinerman, Comp. Phys. Com. **39**, 155 (1986).
[37] D. A. Varshalovich, A. N. Moskalev, and V. K. Khersonskii, *Quantum Theory of Angular Momentum* (World Scientific, Singapore, 1988).